Evolution of micrometeorological observations: Instantaneous spatial and temporal surface wind velocity from thermal image processing

B. Schumacher*[1], M. Katurji[1], J. Zhang[1], I. Stiperski[2], and C. Dunker[3]

[1]University of Canterbury, Dept. of Geography, Christchurch, New Zealand

[2]Department of Atmospheric and Cryosphere Sciences, University of Innsbruck, Austria

[3]Rocket Lab, New Zealand

[1]Email: benjamin.schumacher@pg.canterbury.ac.nz

Abstract

Pattern correlation techniques are commonly used in Particle Image Velocimetry studies to calculate tracer particle velocity in fluids or gases. The techniques can be further improved and used to track landscape scale moving thermal patterns in time sequenced infrared images to estimate a spatial advection velocity field.
This study presents a validation and parametric sensitivity test of commonly used image correlation techniques using data produced from a numerical weather model and field observations from a longwave infrared camera. The numerical simulations aimed to create three different wind speed pattern cases to analyze the performance of four different image velocimetry techniques and compare the estimated velocity field to the model's velocity field. A sensitivity test was carried out with various combinations of required user input to find the best performing image velocimetry techniques. These were then applied to a dataset of surface temperature of an artificial hockey turf field taken with an infrared (IR) camera to test the algorithms in real world conditions and to directly compare the estimated velocity to in-situ measured wind velocity.
The velocimetry algorithms are especially accurate when there is low complexity in ow structure (root mean square error: 0.4: Structural Similarity: 0.81). The comparison of the IR image velocimetry with the in-situ measurements on the hockey turf field shows accurate representation of the 10 minute mean wind direction and the mean wind speed with a maximal absolute error of 0.8 for the wind direction. If the comparison is done on a one minute average basis the accuracy of the image velocimetry decreases when the wind speed drops.

Keywords: Image Velocimetry, Thermal Image Velocimetry, TURF T1 experiment.

*

1 Introduction

Digital image pattern correlation techniques are widely spread in computer vision and spatial flow visualization studies. The correlation techniques are commonly used as a core algorithm in Particle Image Velocimetry (PIV) studies to visualize tracer particle movement in gases or fluids through the image correlation of time sequenced images from illuminated particles (Adrian, 1991; Adrian et al., 2000; Kompenhans et al., 2007). The application of image pattern correlation techniques to derive near surface flow velocity in outdoor field settings is relatively new (Takimoto et al., 2011; Inagaki et al., 2013). Inagaki et al. (2013) applied a PIV correlation technique from Kaga et al. (1992) to infrared images of a hockey turf field to spatially visualize wind velocity. This proved that image correlation techniques can retrieve velocity fields from temperature perturbation patterns within time sequenced thermal images. However computer vision processing algorithms provide various alternatives to Kaga et al.'s (1992) correlation approach. Additionally the image correlation algorithms are highly dependent on user input and experience to retrieve accurate measurements. In the process of developing optimal parametric settings for the four methods this study examines which correlation approach is optimal for the retrieval of velocity fields from moving patterns in sequential images and how user-dependent input can be optimized to retrieve accurate spatial velocity fields under a variety of complex spatio-temporal image property gradients.

Accurate spatial velocity fields are vital for micrometeorological model validation, for estimating spatial distribution of surface-atmosphere energy flux and the development of new atmospheric turbulence theories. Additionally the spatial measurement of wind velocity from infrared images has many practical applications from near-target agricultural meteorology (Katurji and Zawar-Reza (2016)) to field sport events where spatial wind structure is important (van Hooff et al. (2011)).

In PIV studies various tests of correlation techniques were carried out to achieve correct particle displacement estimations for micrometeorological spatial velocity measurements. Kaga et al. (1992) proposed to use the greyscale difference and Gui and Merzkirch (1996) the minimum quadratic difference of interrogation windows to estimate velocity vectors. When two sequenced images are used to estimate particle displacement an interrogation window is a small squared area in both images of

user predefined size. In Image 1 the interrogation window is static whereas in Image 2 it is displaced within a user predefined area. The commonly used interrogation window correlation method is the cross-correlation (CC). According to Kompenhans et al. (2007) all mentioned methods are similarly accurate when applied in a PIV process. However these techniques have not been compared using either artificial moving patterns from numerical model output or sequenced thermal imagery. The spatial measurement of velocity fields for micrometeorological research has been accomplished by smoke visualization and comparison to wind tunnel PIV measurements by Hommema and Adrian (2003). Takimoto et al. (2011) compared wind tunnel CC-PIV measurements and to an urban flow model to characterise urban turbulent flow. Another methodology of measuring outdoor velocity fields is the use of arrays of sonic anemometers (Porte-Agel et al., 2001; Inagaki and Kanda, 2010). The arrays are used to spatially estimate heat flux and enerergy dissipation. The shortcomings of these methods are the high workload for the smoke visualization, the flow distortion through the physical sonic anemometer array and its low resolution due to point measurement sources.

The objective of this study is to develop and test time sequential image velocimetry methods at spatial and temporal scales that make them relevant to micrometeorological applications. We analyzed the performance of three standard image correlation techniques and propose a fourth correlation technique, which uses the structural similarity of the interrogation windows. To assess the accuracy of each correlation technique under changing user input of interrogation window sizes, overlaps and search area sizes a sensitivity test was carried out using the output of a numerical weather model for simulating atmospheric boundary-layer flows at a spatially gridded resolution of 2m. This approach allows for simulating user defined spatial patterns of instantaneous wind speeds that reflect a variety of known structural complexity.

2 Methods and Data

2.1 PALM Model

The Parallelized Large-Eddy Simulation Model (PALM) is a numerical weather model for simulating atmospheric boundary-layer flows. PALM is capable of resolving turbulent flow structures smaller than meso-alpha scale ($\sim$ 200km^2) with spatial resolutions from 200 m to 0.5 m per grid cell

(Maronga et al., 2015). The resolved turbulent flow field can be a result of natural convection caused by solar heating of surface or mechanically induced due to flow separation around wind shear effects and/or obstacles. In this study PALM was mainly used to simulate three different turbulent boundary layers that produced a varying range of spatial complexity required for the analysis:

1. No-Wind: A convective atmospheric boundary layer with very weak background wind speeds that created weak surface wind speeds and a spatial structure with convergence and divergence patterns.

2. Strong-Wind: A wind-forced atmospheric boundary layer imposed on a convective boundary layer that created high wind speed gusts

3. Wake-Wind: A turbulent wake produced by vortices being shed in the lee of a cuboid producing oscillating waves of various windspeeds.

Four different image correlation techniques in various pre-defined user input cases were then applied to two consecutive PALM simulated windspeed images to calculate the advection wind velocity field. Then the retrieved advection velocity field was compared to the PALM velocity field. This sensitivity test was carried out to optimize and test our image pattern correlation algorithms prior to the application on infrared imagery.

PALMs numerical domain was set up for all three cases with a resolution of dx=dy=dz= 2 meter where the x direction is base for the u and the y direction is base for the v velocity (See Figure 1). The domain was set up with a vertical stretch to a larger spacing above 100 meter for the NoWind and StrongWind cases, above 150 meter for the Wake-Wind case. For the NoWind and StrongWind case a convective boundary layer with solar radiation of southern hemisphere summertime at 43°S (12 pm Christchurch) was used. The Wake-Wind case was set up with no radiation process. At x = 70m, y = 160 m a 20 by 20 by 100 meter block was set to create the turbulent wake for the Wake-Wind case. In the NoWind and the StrongWind case a cyclic boundary condition was set following standard methodologies in these types of simulations (Tabor and Baba-Ahmadi, 2010). The models simulation time was set to 3600 seconds for all cases. Further information about the model setup can be found in Table 1.

PALM was set up in three different cases as explained above with increasing complexity of flow structure. The complexity of the flow structure is defined by the advection velocity in one direction (See Fig 1 a)), the convergence and divergence patterns (See Fig 1 b)) and the wake shedding and creation of reverse flow (See Fig 1 c)). Therefore the lowest complexity is found in the StrongWind case with initial wind only in u direction and evolving convection (See Fig 1 a)). A more complex case is a very low wind with strong convection (See Fig 1 b)). The highest complexity was reached through the Wake-Wind case (See Fig 1 c)).

Table 1: PALM further model setup information

Case Name	Initial wind speed	Initial potential temperature	Boundary condition	domain size (x*y*z)m
StrongWind	4.0 m/s surface increasing to 6 m/s at 100m	293K at surface build up to 296K at 350m, same after 350m	Cyclic boundary (x and y)	1024 * 512 * 1574
NoWind	0.1 m/s at all levels in x direction	293K at surface build up to 296K at 350m, same after 350m	Cyclic boundary (x and y)	1024 * 512 * 1574
Wake-Wind	4.0 m/s at all levels in x direction	293.15K at all levels	Cyclic boundary (y) open boundary (x)	1280 * 320 * 1084

2.2 Image Correlation Techniques

To produce the advection velocity fields (WSadv) from different image correlation techniques the near-surface (2 m AGL) two dimensional horizontal windspeed was calculated from the PALM u and v wind vector components (see Figure 1). The PALM simulations were allowed to run for 3600 seconds and the resultant wind speed pattern at time = 3542 seconds was used after allowing the model to fully develop the required turbulent boundary layer.

A velocity vector is determined by comparing two interrogation windows of the same user-defined size set in the images. An interrogation window is a raster window of a user-defined size which is moved across Image 1 (Figure 2). For the calculation of one velocity vector the interrogation window in Image 1 is static while the interrogation window in Image 2 is shifted within the user-defined search area size around the interrogation window size. The number of shifts within the search area size is determined by the user-defined overlap of the interrogation window sizes. A higher overlap therefore leads to a longer computation time but increases the probability to find a fitting displacement interrogation window. A larger search area size divides the image into fewer search areas and leads to less initial set interrogation windows because of the higher search radius around each interrogation window. For each displaced interrogation window a comparative metric is

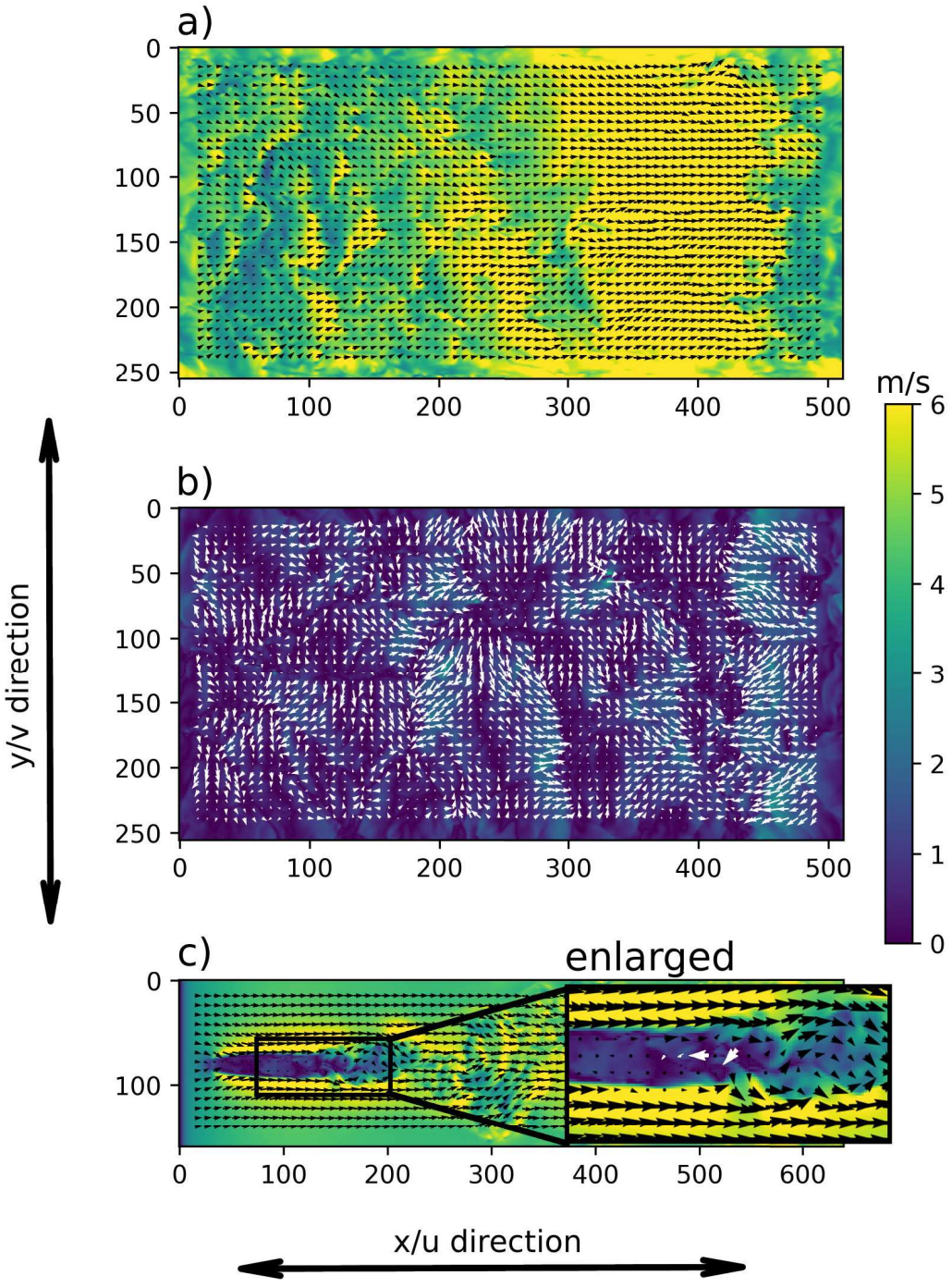

Figure 1: Flow Structure of PALM at 3542 seconds of total 3600 seconds simulation time (view from top on the XY-Plane) for a) StrongWind case b) NoWind case and c) Wake-Wind case. The background color emphasizes the wind speed. The vectors the wind direction. Vector lengths are picked according to the wind speed. White/black colored vectors used for contrast reasons except for the enlarged part in c) where the white arrows emphasize the return flow towards the obstacle in the Wake-Wind case. The black arrows on the side show the directions referred to throughout the manuscript.

calculated to find the window with the maximum correlation (See Figure 2). All correlation values were saved in a correlation matrix to find peak correlation position in reference to the interrogation window in Image 1 (See Figure 2). This peak pixel correlation defines the major advection velocity vector and its direction. Due to a gradient from the peak correlation position to the neighbouring pixels a sub-pixel peak correlation defines a minor direction within the found maximum peak pixel (Kompenhans et al., 2007). Sub-pixel peak positions were calculated through gaussian fitting using the openPIV Python package (Taylor et al., 2010). For the calculation of WSadv four different correlation techniques were tested from which three were previously used in the literature and one new one is presented for this application:

- The cross-correlation method through Fast-Fourier transform which is widely used in Particle Image Velocimetry (Adrian, 1991) (CC-Tech). The cross-correlation determines a correlation matrix between two interrogation windows and finds the pixel that correspond to the peak correlation (Kompenhans et al., 2007).

- The grey-level difference method which was used for Thermal Image Velocimetry (Inagaki et al., 2013; Kaga et al., 1992) (Greyscale-Tech). This method uses the minimum accumulated absolute difference of the interrogation windows to find the pixel of displacement.

- The minimum Quadratic difference (MQD) of the interrogation windows(Gui and Merzkirch, 1996) (SQM-Tech). This method uses the minimum squared difference of the interrogation windows to find the pixel of displacement.

- The Strucual Similarty measure(SSIM) of the interrogation windows which was newly evaluated using this context (SSIM-Tech). This method finds the maximum SSIM value of the interrogation windows to find the pixel of displacement. For more information about SSIM refer to Wang et al. (2004).

The impact of the window size, search area size and window overlap was tested in a sensitivity test to find the optimal parameter settings and correlation technique. SQM-Tech although similar to Greyscale-Tech was added to the analysis to have a comparison to the performance of Greyscale-Tech. Greyscale-Tech builds on the difference of the values of the interrogation windows whereas SQM-Tech uses the square root of the squared difference. Therefore SQM-Tech has the possibil-

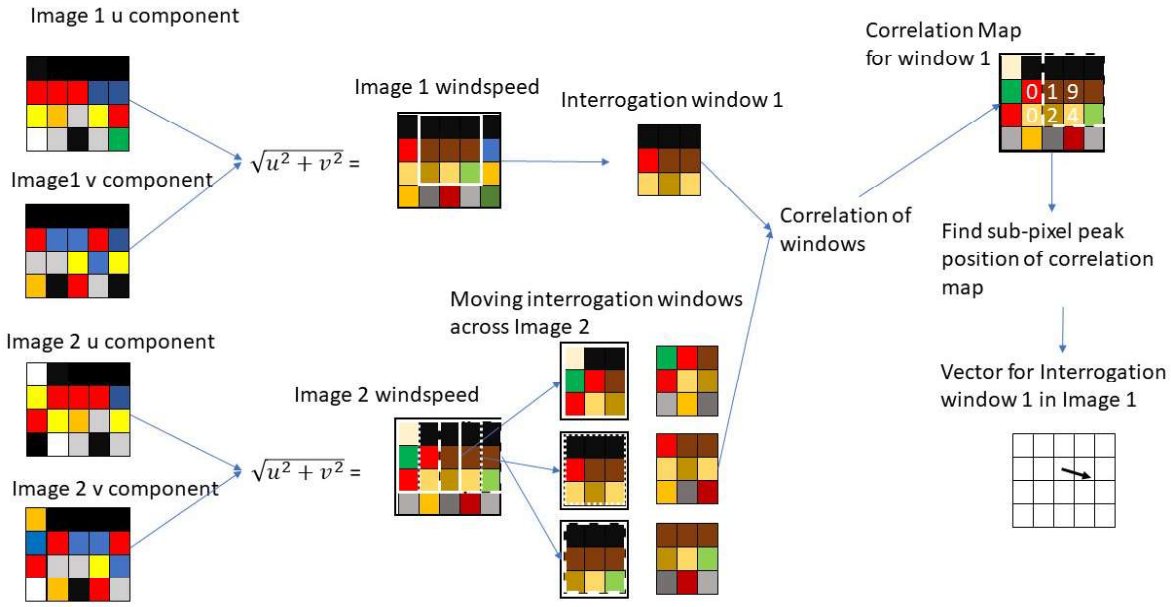

Figure 2: Conceptual diagram summarizing the steps required for determining advection velocities from image correlation techniques 2-4. The preprocess of calculating windspeed images from PALM is included. The concept of CC-Tech is slightly different and can be found in Kompenhans et al. (2007)

ity to increase accuracy compared to Greyscale-Tech due to the increase of weight on large pixel differences. SSIM-Tech is well-known in the image processing community but to the authors knowledge has not been used for image velocimetry correlation. It is mainly accounting for structural inter-dependencies of pixels whereas the other techniques estimate absolute errors (Wang et al., 2004).

2.3 Sensitivity test and accuracy assessment

According to Kompenhans et al. (2007) the success of image velocimetry depends on the user determined overlap and window size. Therefore a sensitivity test of all PALM cases and all correlation techniques was carried out using various window sizes, search area sizes and window overlaps (see Table 2). The various overlaps were picked according to the minimum reccomended overlap of 50 % (Kompenhans et al., 2007). The search area sizes were selected values within 1.5 * window size to 3 * window size. This created 1377 velocity field comparisons. These were qualitatively assessed using the vector images and quantitatively analysed using the root mean square error (RMSE) and the Structual Similarty Measure (SSIM). The best performing algorithms were applied to the field experiment dataset descibed in section 2.4.

Table 2: Tested combinations of window sizes, overlaps and search area sizes. window and search area size indicates the number of pixels in one side of a square.

Window size	**Overlaps**	**Search area sizes**
8	7, 6, 5, 4	12, 16, 24, 32
12	11, 10, 9, 8, 7, 6	18, 24, 32, 36
16	15, 14, 13, 12, 11, 10	20, 24, 32, 40, 48
24	23, 22, 21, 20, 19, 18	30, 36, 48, 56, 72
36	35, 34, 33, 32, 31, 30, 29, 28, 27, 26, 25, 24, 18	42, 54, 72
48	47, 45, 41, 40, 36, 32, 30, 24	64, 72

2.4 TURF-T1 Data and Analysis

The Time seqUential theRmal inFrared-Turbulence (TURF T1) was a field campaign carried out on an artificial hockey field (50 by 100 meters) in Rangiora, New Zealand in January 2019. The goal of this field campaign was to develop precise image velocimetry techniques that are suitable for landscape scale near surface mean and turbulent wind velocity. TURF T1 with its homogenous surface cover type, lack of surface moisture and homogeneous roughness provides optimal conditions to develop this methodology. Additionally the work is highly comparable to previous study from Inagaki et al. (2013) and Christen et al. (2012). The sonic anemometers were placed on one tower 0.5 (IRG1) and 1.5 (IRG2) meter above ground (see Figure 3 B)). The 3-dimensional wind velocity measurements were carried out at 60 Hz and averaged to 20Hz by the data logger and were synchronized with a GPS clock to match the aerial infrared acquisition. Sonic anemometer data were tilt corrected with the planar fit method to address uncertainties in the orientation of the sonic anemometers (Wilczak et al., 2001). In this experiment with flat terrain a wind velocity extrapolation was carried out to estimate the very-near surface wind velocity by the usage of the logarithmic wind profile. This assumes a neutrally stratified atmosphere which will be analyzed using the two sonic anemometers. For the logarithmic profile conversion a height of 1.5 cm and a roughness length parameter Z_0 of 0.01m was used (Stull, 2011).

The infrared dataset was collected using an unmanned aerial quadcopter flying at a height of 60 meter above the surface equipped with an Optris Infrared Camera (PI450, resolution: 640 x 480 pixels) using a wide angle lens (80°x 54°). Due to the battery life of the Quadcopter a single experiment time was limited to around 10 minutes. A total of five experiments were carried out. At the time of the experiments the weather was partly cloudy with a north easterly wind with a mean wind speed of 1.3 m/s and around 22 °C air temperature. The thermal images were retrieved at a frequency of 80 Hz. In the preprocessing phase the images were subsampled to 1 Hz to allow enough temperature change between sequential images. Despite the use of an inertial stabilizer (3-axis gimbal) there appeared to be residual image shaking that was taken out with subsequent software-based stabilization. In order to stabilize the numerical temperature values the original, shaky raster data was converted to RGB color raster images. Then the images were stabilized in RGB color values using Blender (Blender Online Community, 2019). To retrieve the temperature values back

from the stabilized images a random forest model was trained on each original temperature RGB color values image pair. The stabilized RGB color images were used as a predictor to retrieve back stable temperature value rasters. To use the infrared imagery in the developed velocimetry algorithms Inagaki et al. (2013) suggested high pass filter should be applied for each local time series (pixel) of the infrared imagery. The high pass filter highlights the anomalous temperature pattern perturbations that are induced by the near-surface actual wind velocity and solar heating. The resulting temperature perturbations reveal moving patterns which can be tracked.

Based on the SSIM value the most successful window size - overlap - search area size combinations of the PALM sensitivity test were obtained and used for the image velocimetry calculation of the infrared imagery (see Table 3). The comparison of the image velocimetry and the sonic anemometer data was carried out using a 5 by 5 matrix of vectors closest to the position of the sonic anemometer tower. Each of these vectors refer to one fixed interrogation window in space and therefore are seen as an independent, virtual velocity measurement from image velocimetry. The 25 closest vectors were picked because the lowest available resolution allowed to retrieve a set of vectors close to the sonic anemometers. We refer to the comparison of each of the 25 image velocimetry vectors to the sonic anemometer as single vector comparisons. From each of the 25 vectors the 10 minute wind vector average was calculated and compared to the 10 minute extrapolated mean of IRG2. On a higher frequency domain of 1 minute the prevailing wind direction of IRG2 was scattered in a sector of +/-30°in wind direction. Therefore the best performing 10 minute single vector comparisons were defined to lie in an accuracy range of +-30 °of the IRG wind direction mean. To analyze the vector performance in a higher frequency a one minute mean was applied to the best performing 10 minute mean single vector comparisons. The one minute mean image velocimetry wind speed and wind direction vectors were then compared to the extraploated near-surface one minute mean wind velocity of IRG2 in a single vector comparison as well.

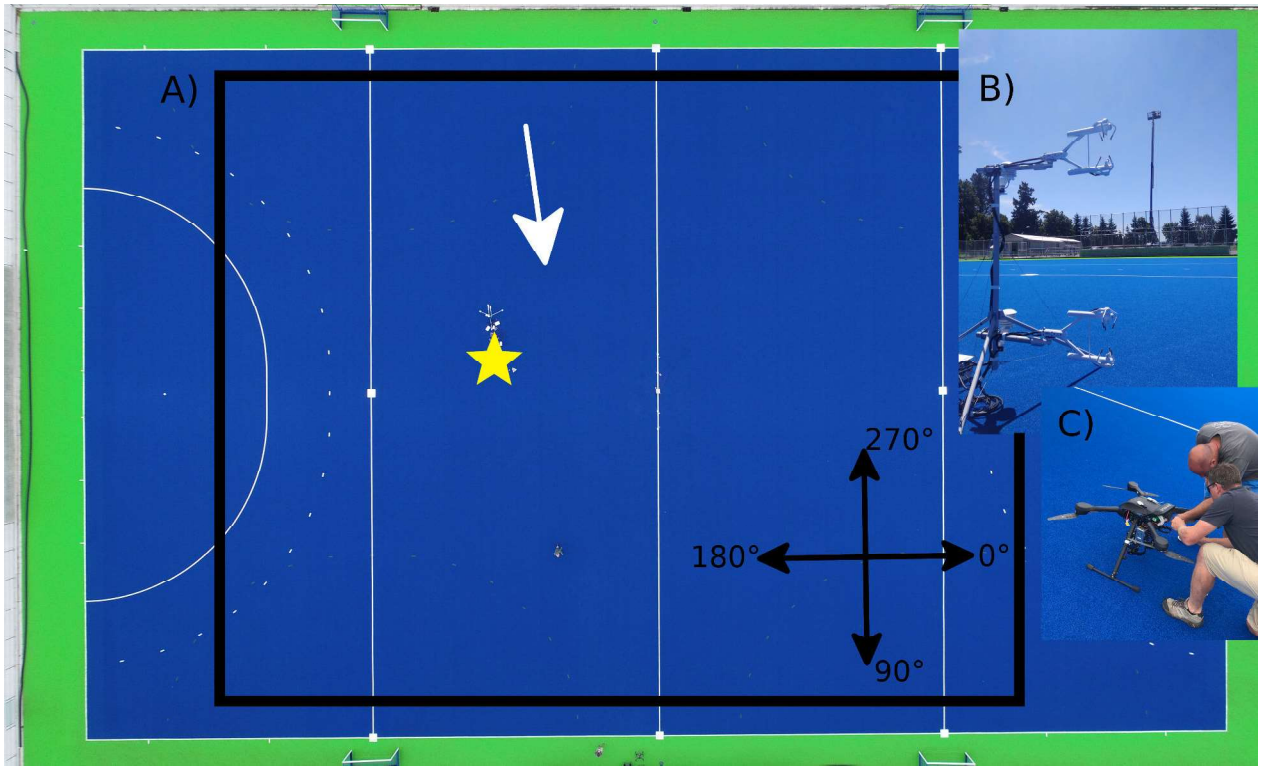

Figure 3: A) Picture of TURF T1 experiment on a hockey turf field. White arrow indicates mean main wind direction. The yellow star shows the position of the sonic anemometer tower. The black square emphasizes the footprint of the thermal imagery. The black arrows show the wind direction coordinate system. B) side view on the sonic anemometer tower C) Quadcopter with Optris infrared cameras

3 Results and Discussion

3.1 PALM Sensitivity Test

The sensitivity tests enabled the qualitative and quantitative analysis of the velocity fields created by the four different image correlation techniques and its various combinations of window sizes, overlaps and search area sizes. The number of vectors decreases with increasing window size, limiting the number of vectors available for analysis when larger search areas are used. This created some unuseful cases in the smaller Wake-Wind case domain which were eliminated.

A direct comparison between the derived advection velocity and the models velocity shows similar wind patterns in all cases (see Fig 4a) b) and c)). Furthermore the determined wind speed is comparable with the model's wind speed.

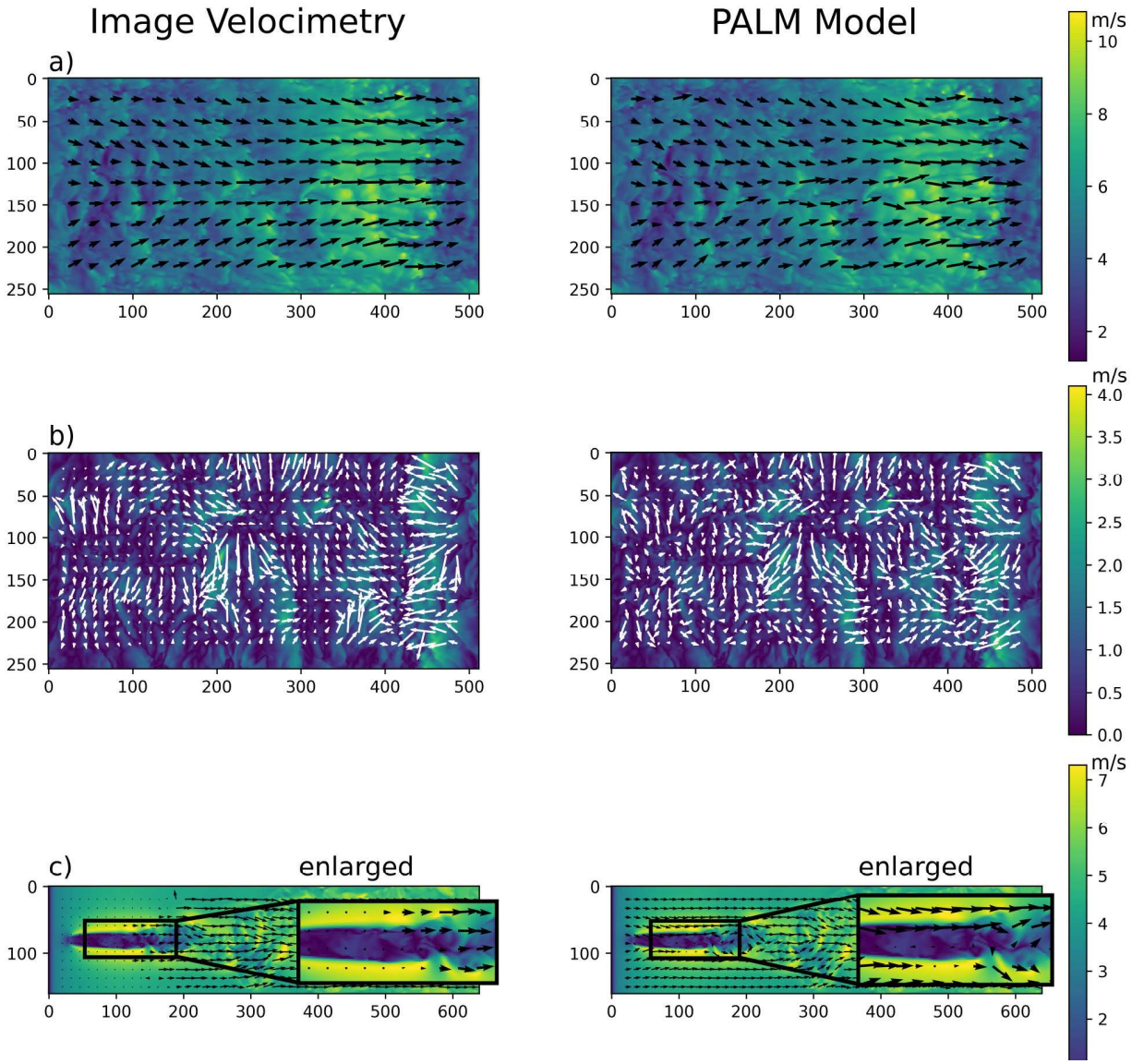

Figure 4: Direct comparison of greyscale image velocimetry technique for a) StrongWind case b) NoWind case and c) Wake-Wind case. The white arrows in b) are only used for contrast reasons. The enlarged part in c) clearly shows the inaccuracy of the image velocimetry in the Wake-Wind case in the lee area of the obstacle.

Evaluation metrics showed that the highest SSIM comparison values could be reached in the Strong-Wind case followed by the NoWind case and the Wind-Wake case. The highest SSIM value and the lowest RMSE value was reached by Greyscale-Tech. It is evident that for Greyscale-Tech, SQM-Tech and SSIM-Tech the maximum available overlap is creating the most accurate image velocimetry pattern (see Table 3). The analysis suggests that the optimal overlap for CC-Tech is ∼3/4 of the window size. The reason for this can be found in the slightly different working mechanism which directly correlates the search area with the interrogation window. A larger overlap will create more autocorrelations between neighbouring vectors in CC-Tech and the chance for error vectors is increased. This is traditionally not the case when using the cross-correlation on illuminated particle images where illuminated peak pixels are available. However the images in this study do not provide such illuminated pixels. Therefore the PIV CC-Tech algorithm is creating the lowest accuracy in this analysis (see Table 3).

Table 3: Best perfoming image velocimetry algorithms for each case - correlation technique combination

Method	**Case**	**Window Size**	**Overlap**	**Search Area Size**	**SSIM**	**RMSE**
CC-Tech	StrongWind	36	25	42	0.61	1.36
Greyscale-Tech	StrongWind	24	23	48	0.82	0.58
SQM-Tech	StrongWind	16	15	40	0.81	0.66
SSIM-Tech	StrongWind	24	23	56	0.81	0.61
CC-Tech	NoWind	36	24	42	0.39	0.74
Greyscale-Tech	NoWind	24	23	56	0.77	0.37
SQM-Tech	NoWind	36	35	54	0.74	0.42
SSIM-Tech	NoWind	24	23	56	0.74	0.38
CC-Tech	Wake-Wind	8	7	16	0.25	1.26
Greyscale-Tech	Wake-Wind	24	23	48	0.5	1.06
SQM-Tech	Wake-Wind	24	23	48	0.52	1.03
SSIM-Tech	Wake-Wind	24	23	48	0.52	1.03

3.2 TURF-T1

The TURF-T1 experiment dataset enabled the application of the image velocimetry algorithms to an infrared dataset and its comparison to in-situ measurements. The comparison of the 10 minute mean vectors close to the sonic anemometer show similarities in all tested cases (see Table 4). The algorithm with the lowest combined relative error in wind speed and wind direction for the 10-

minute mean comparison was a vector of Greyscale-Tech (window size: 16 , overlap: 15, SA: 32; see Table 4). All other techniques provided very accurate single vector comparisons as well. Most of the other single vector comparison inaccuracies were manifested in a large wind speed error. This error depends largely on the estimation of the logarithmic wind profile which was not properly assessed in this experiment. Therefore the error in wind direction is more informative.

For the one minute mean all available 10-minute mean cases within +-30° accuracy in wind direction were tested. The result shows acceptable accuracy for the wind direction with CC-Tech, Greyscale-Tech and SQM-Tech. In the qualitative analysis CC-Tech is producing distinctly more error vectors then Greyscale-Tech and SQM-Tech. Therefore the analysis was focused on Greyscale-Tech and SQM-Tech. The accuracy of the 1 minute mean wind direction of Greyscale-Tech stands out in Minute 1 - Minute 3 and Minute 5 - Minute 8 (see Table 5). Especially in Minute 4 and Minute 9 when the wind speed evidently drops the Image Velocimetry algorithm is not capable of delivering correct wind directions (see Table 5 red numbers). This might be connected to the nature of the artificial hockey turf which can cause a thermal inertial delay through the capability of storing thermal energy for a short period of time in a heating phase when the winds are weak.

Table 4: Best 10-minute mean single vector Image Velocimetry to sonic anemometer comparisons for all correlation techniques.

Method	**Window Size**	**overlap**	**Search Area Size**	**Mean WD**	**Mean WS**	**Absolut Error WD**	**Absolut Error WS**	**Relative error WD**	**Relative error WS**
$IRG2\_log$				87.07	0.11	0	0	0	0
$Greyscale - Tech$	16	15	32	87.87	0.11	0.8	0.0	0.9%	1.0%
$SSIM - Tech$	16	15	20	86.47	0.11	−0.60	0.002	1.05%	1.75%
$CC - Tech$	16	15	32	88.74	0.10	1.67	0.005	1.9%	5.1%
$SQM - Tech$	16	14	24	73.69	0.11	−13.38	0.001	15.36%	0.7%

Table 5: One minute mean comparison of IV to sonic anemometer.

Variable	**Method**	**Min 1**	**Min 2**	**Min 3**	**Min 4**	**Min 5**	**Min 6**	**Min 7**	**Min 8**	**Min 9**	**Min 10**	**Window Size**	**Overlap**	**Search Area Size**	**RMSE**
ws	$IRG2$	3.07	2.75	2.47	1.69	3.37	3.15	3.08	2.72	1.31	2.70				
ws_log	$IRG2log$	0.25	0.22	0.2	0.14	0.27	0.26	0.25	0.22	0.11	0.22				
wd	$IRG2$	96.29	15.09	73.39	123.22	82.82	94.51	83.79	39.8	112.81	115.87				
ws	$greyscale$	0.2	0.28	0.21	0.49	0.18	0.16	0.33	0.35	0.33	0.32	16	15	32	0.15
wd	$greyscale$	86.03	40.64	49.76	79	103.57	90.94	106.41	70.53	81.76	94.01	16	15	32	25.72
ws	$Cross - correlation$	0.14	0.05	0.07	0.12	0.09	0.09	0.02	0.01	0.03	0.07	36	25	42	0.16
wd	$Cross - correlation$	111.74	82.46	90.13	93.08	95.52	87.65	110	59.93	96.31	117.46	36	25	42	27.46
ws	SQM	0.55	0.46	0.39	0.32	0.26	0.24	0.46	0.27	0.22	0.18	24	23	36	0.17
wd	SQM	83.02	87.97	95.49	94.46	77.14	89.83	83.93	75.43	82.93	92.64	24	23	36	30.92
ws	$SSIM$	0.09	0.04	0.11	0.08	0.33	0.06	0.04	0.04	0.08	0.04	16	15	32	0.15
wd	$SSIM$	35.36	66.78	21.3	42.64	166.24	97.02	86.3	61.62	146.51	122.56	16	15	32	49.21

The wind speed drop can be noticed in the one minute mean streamline plots as well (see Figure 5). It is evident that especially in low wind phases there are not enough images to track the wind pattern footprint. Additionally, the streamline plots show divergence and convergence patterns which indicate cooling phases through divergence fields and heating phases through convergence fields. The assessment of these phenomena will need further analysis and data and a more adaptive algorithm towards the size and shape of the coherent flow structures and the inertial thermal delay of the surface type. Furthermore the current image velocimetry algorithms create unequal numbers of velocity vectors due to different search area sizes. The goal here is to find an intelligent algorithm to adapt the image velocimetry towards a continuous time/space velocity coverage.

4 Conclusion and Outlook

In this paper we presented a comparison of four different image velocimetry techniques which were applied to an artificial, 2-dimensional wind velocity pattern to find the optimal algorithms for the application to a thermal infrared dataset comparable to Inagaki et al. (2013). It is evident that all velocimetry techniques can successfully retrieve wind velocity fields from the artificial velocity patterns. The cross-correlation technique, commonly used in PIV, is not as accurate as the other tested techniques. The main reason for this might be the creation of more error vectors and the missing illumination peak pixels which are typical for the use case of the PIV images. Although the CC-Tech has been widely tested with illuminated particle images, hence we further recommend using it for PIV. An overall recommendation for the usage of the image velocimetry techniques can be found in Table 6.

Table 6: Correlation technique recommendation

Method	**Cases recommended for**
CC-Tech	PIV/illuminated particle images
Greyscale-Tech	StrongWind/ NoWind/ infrared images
SQM-Tech	StrongWind/ NoWind/ WakeWind/ infrared images
SSIM-Tech	StrongWind/NoWind/WakeWind/ infrared images

Furthermore the application to the infrared dataset from the Time seqUential theRmal inFrared-Turbulence (TURF T1) campaign agreed well with the sonic anemometer measurements within 1%

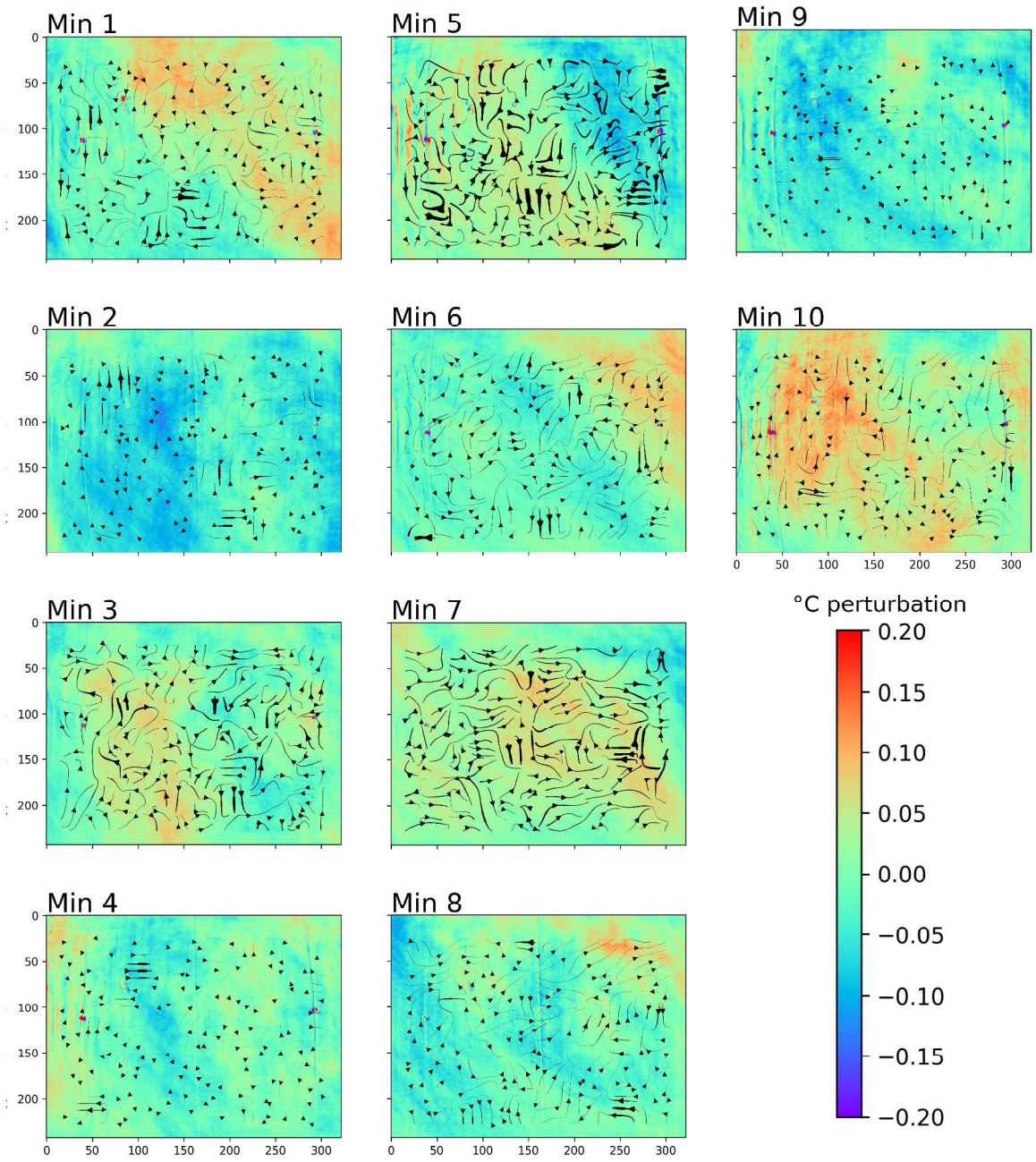

Figure 5: Minutely mean of temperature pertubations including wind patterns. Evident is the wind speed drop in Min 4 and Min 9 and the wind speed increase in Min 5.

relative error for the best performing correlation technique in the 10 minute mean wind speed and direction comparison. The most successful combination of window size, overlap and search area sizes for this use case was 16/15/32 with the greyscale correlation technique. The one minute mean comparison of the Image Velocimetry and the sonic anemometers shows that with weak winds the image velocimetry algorithm can not cover the wind direction properly. This might be connected to a thermal inertial delay of the artificial hockey turf field which is capable of storing energy over a short period of time and creating a time response lag in subsequent infrared images. This will be further assessed in future studies to better extract the turbulent wind information.

Further work with the TURF T1 dataset will allow better assessment of the accuracy and performance of the turbulent spatial velocity field especially in higher frequency domains through the application of high order statistics on the infrared velocimetry. Additionally further development of the image correlation techniques will lead to a higher resoluted image velocimetry. Other TURF T1 experiments were additionally equipped with a near surface thermocouple array which allows the closer assessment of surface-atmospheric turbulent fluxes their spatial measurement. Lastly we aim to validate the existing footprint models for sonic anemometers with the spatial image velocimetry technique.

5 Acknowledgements

This work was carried out under the framework of the research program "The invisible realm of atmospheric coherent turbulent structures: Resolving their dynamics and interaction with the Earths surface" which was funded by the Royal Societyof New Zealand with contract number RDF-UOC1701. We want to express special thanks to Justin Harrison, Paul Bealing and Nicholas Key who helped with the TURF experiment and the UAV operations.

6 References

Adrian, R.

1991. PARTICLE-IMAGING TECHNIQUES FOR EXPERIMENTAL FLUID-MECHANICS. *AN-*

NUAL REVIEW OF FLUID MECHANICS, 23:261–304.

Adrian, R., C. Meinhart, and C. Tomkins

2000. Vortex organization in the outer region of the turbulent boundary layer. *JOURNAL OF FLUID MECHANICS*, 422:1–54.

Blender Online Community

2019. *Blender - a 3D modelling and rendering package*. Blender Foundation, Blender Institute, Amsterdam.

Christen, A., F. Meier, and D. Scherer

2012. High-frequency fluctuations of surface temperatures in an urban environment. *THEORETICAL AND APPLIED CLIMATOLOGY*, 108(1-2):301–324.

Gui, L. C. and W. Merzkirch

1996. A method of tracking ensembles of particle images. *Experiments in Fluids*, 21(6):465–468.

Hommema, S. and R. Adrian

2003. Packet structure of surface eddies in the atmospheric boundary layer. *BOUNDARY-LAYER METEOROLOGY*, 106(1):147–170.

Inagaki, A. and M. Kanda

2010. Organized Structure of Active Turbulence Over an Array of Cubes within the Logarithmic Layer of Atmospheric Flow. *BOUNDARY-LAYER METEOROLOGY*, 135(2):209–228.

Inagaki, A., M. Kanda, S. Onomura, and H. Kumemura

2013. Thermal Image Velocimetry. *BOUNDARY-LAYER METEOROLOGY*, 149(1):1–18.

Kaga, A., Y. Inoue, and K. Yamaguchi

1992. Application of a Fast Algorithm for Pattern Tracking on Airflow Measurements. . *Tanida Y., Miyashiro H. (eds) Flow Visualization VI.*

Katurji, M. and P. Zawar-Reza

2016. Forward-Looking Infrared Cameras for Micrometeorological Applications within Vineyards. *SENSORS*, 16(9).

Kompenhans, J., M. Raffel, S. T. Wereley, and C. E. Willert
2007. *Particle image velocimetry : a practical guide ; with 42 tables.* Springer.

Maronga, B., M. Gryschka, R. Heinze, F. Hoffmann, F. Kanani-Suehring, M. Keck, K. Ketelsen, M. O. Letzel, M. Suehring, and S. Raasch
2015. The Parallelized Large-Eddy Simulation Model (PALM) version 4.0 for atmospheric and oceanic flows: model formulation, recent developments, and future perspectives. *GEOSCIENTIFIC MODEL DEVELOPMENT*, 8(8):2515–2551.

Porte-Agel, F., M. Pahlow, C. Meneveau, and M. Parlange
2001. Atmospheric stability effect on subgrid-scale physics for large-eddy simulation. *ADVANCES IN WATER RESOURCES*, 24(9-10):1085–1102.

Stull, R.
2011. *Meteorology for Scientists and Engineers, 3rd Edition.*, 3rd edition. Univ. of British Columbia.: Univ. of British Columbia.

Tabor, G. R. and M. H. Baba-Ahmadi
2010. Inlet conditions for large eddy simulation: A review. *COMPUTERS & FLUIDS*, 39(4):553–567.

Takimoto, H., A. Sato, J. F. Barlow, R. Moriwaki, A. Inagaki, S. Onomura, and M. Kanda
2011. Particle Image Velocimetry Measurements of Turbulent Flow Within Outdoor and Indoor Urban Scale Models and Flushing Motions in Urban Canopy Layers. *BOUNDARY-LAYER METEOROLOGY*, 140(2):295–314.

Taylor, Z. J., R. Gurka, G. A. Kopp, and A. Liberzon
2010. Long-Duration Time-Resolved PIV to Study Unsteady Aerodynamics. *IEEE TRANSACTIONS ON INSTRUMENTATION AND MEASUREMENT*, 59(12):3262–3269.

van Hooff, T., B. Blocken, and M. van Harten
2011. 3D CFD simulations of wind flow and wind-driven rain shelter in sports stadia: Influence of stadium geometry. *BUILDING AND ENVIRONMENT*, 46(1):22–37.

Wang, Z., A. Bovik, H. Sheikh, and E. Simoncelli

2004. Image quality assessment: From error visibility to structural similarity. *IEEE TRANSACTIONS ON IMAGE PROCESSING*, 13(4):600–612.

Wilczak, J., S. Oncley, and S. Stage

2001. Sonic anemometer tilt correction algorithms. *BOUNDARY-LAYER METEOROLOGY*, 99(1):127–150.